EVALUATION OF LIQUEFACTION POTENTIAL OF ROCK DEBRIS USING ENERGY BASED METHOD

M. Sawatsubashi [1], M. Ishimaru [2], K. Hiraga [3], S. Nakamura [4]

[1] *Research Associate, Central Research Institute of Electric Power Industry, Civil Engineering Research Laboratory, Earthquake Engineering Sector, Chiba, Japan, sawatsubashi3761@criepi.denken.or.jp*

[2] *Researcher, Central Research Institute of Electric Power Industry, Civil Engineering Research Laboratory, Earthquake Engineering Sector, Chiba, Japan, ishimaru@criepi.denken.or.jp*

[3] *Engineer, Civil Engineering Research & Environmental Studies, Inc., Chiba, Japan, hiraga@ceresco.jp*

[4] *Senior Manager, JPOWER, Nuclear Power Engineering Dept, Civil Engineering Office, Tokyo, Japan, satoshi_nakamura@jpower.co.jp*

Abstract

Liquefaction assessment is necessary to evaluate the seismic stability of ground foundations for Class S facilities under new regulatory requirements for nuclear power plants. The evaluation of the liquefaction potential of rock debris or gravelly soil, conventionally regarded as non-liquefiable soil, is necessary since standard ground motion becomes stronger. The number of element tests of rock debris, however, is limited. Moreover, previous studies noted that the conventional F_L method using the stress-based method cannot evaluate the post-liquefaction behavior and underestimate the liquefaction resistance of rock debris. Recently, the energy-based method for liquefaction potential evaluation has been proposed to accurately evaluate post-liquefaction deformation. In this study, a series of undrained cyclic loading tests were conducted for rock debris using a large triaxial apparatus (300 mm in diameter and 600 mm in height) in order to clarify the applicability of the energy-based method to rock debris. The results demonstrate the applicability of the energy-based method to rock debris; the excess pore water pressure ratio was nearly 1 when the normalized accumulated dissipated energy was in the range of 0.02–0.04 and the result from the proposed equation for liquefaction resistance using the stress-based method ($N_c = 20$, $\varepsilon_{DA} = 5\%$) and the normalized accumulated dissipated energy based on element tests with sandy soil was almost consistent with the result obtained from the tested rock debris. The normalized accumulated dissipated energy at the liquefaction state ($\varepsilon_{DA} = 5\%$) increased as N_c increased. The increase in ε_{DA} for the normalized accumulated dissipated energy was small compared with that of sandy soil. The effect of the confining pressure on rock debris was almost negligible. The relationship between the normalized accumulated dissipated energy and the shear modulus ratio depends on the cyclic stress ratio even when normalization was performed. The volumetric strain as a result of reconsolidation after liquefaction (ε_v) had a stronger relationship with the normalized accumulated dissipated energy compared with the maximum shear strain (γ_{max}). This indicates that the energy-based method can evaluate the post-liquefaction behavior of rock debris more accurately. This study will improve the applicability of the energy-based method to rock debris and the evaluation of the post-liquefaction behavior of the material.

Keywords: Rock debris; Liquefaction; Accumulated dissipated energy; Large triaxial test

1. Introduction

Liquefaction assessment is necessary to evaluate the seismic stability of ground foundations for Class S facilities under new regulatory requirements for nuclear power plants. The evaluation of the liquefaction potential of rock debris, conventionally regarded as non-liquefiable soil, is necessary since standard ground motion becomes stronger. Liquefaction of rock debris avalanche was reported during the 1993 Hokkaido-Nansei-Oki earthquake [1]. Liquefaction of gravelly fills was also observed during the 1995 Hyogo-ken Nanbu earthquake [2]. Hara [3] found that well-graded granular soil is liquefiable like poorly graded sand. On the other hand, the post-liquefaction undrained monotonic shear strength of well-graded granular soil is much higher than that of poorly graded sand, which indicates that large deformation is unlikely to occur in the liquefaction of well-graded granular materials. The conventional F_L method using the stress-based method, which evaluates the liquefaction potential by comparing the liquefaction strength of soil and the cyclic shear stress, cannot be employed to evaluate the post-liquefaction behavior as it underestimates the liquefaction resistance of rock debris. However, the number of element tests in the liquefaction characteristics of rock debris is still limited.

Recently, an energy-based liquefaction evaluation method has been proposed. In this method, the accumulated dissipated energy is calculated using the enclosed area of the hysteresis loop of the stress–strain relationship obtained from an undrained cyclic loading test. The accumulated dissipated energy is compared with the energy produced as a result of an earthquake to evaluate the liquefaction potential. Towhata and Ishihara [4] conducted an experimental study and found a unique correlation between the excess pore water generation and the accumulated dissipated energy per unit volume during undrained cyclic loading tests with different shear stress histories. Similar results were also reported by Ricardo et al. [5]. They also attempted to evaluate the development of shear strain based on the accumulated dissipated energy. However, most existing studies focused on sandy soil, and the applicability of the energy-based method to granular materials such as rock debris has not been clarified.

In this study, a series of large triaxial tests were conducted on rock debris to clarify the applicability of the energy-based method to rock debris. The results of the undrained cyclic loading tests were analyzed in terms of the accumulated dissipated energy normalized by the initial effective mean stress. The volumetric strain generated as a result of reconsolidation after undrained cyclic loading was also measured.

2. Methodology

2.1 Materials

One sample of rock debris was used in this study. Figure 1 shows the particle size distribution and the basic properties of the rock debris. We conducted sieve tests after the undrained cyclic loading test to evaluate the degree of particle breakage since the rock debris can be crushed during the experimental process. The rock debris initially had 6.5% of fine contents (F_c) and 63.6% of gravel contents (G_c). Although the F_c increased by 1.5% after the undrained cyclic loading test, the degree of particle breakage seemed negligible in this study.

The test specimens were prepared by dry tamping to achieve a target dry density (ρ_d) of 1.649 g/cm^3, which is equal to 98% of the degree of compaction (D_c), without causing particle breakage. The samples were divided into sublayers to obtain uniform tamping and prevent particle segregation. Before placing the sample of the next layer, the surface of the previously compacted layer was scratched to ensure good interlocking between adjacent layers.
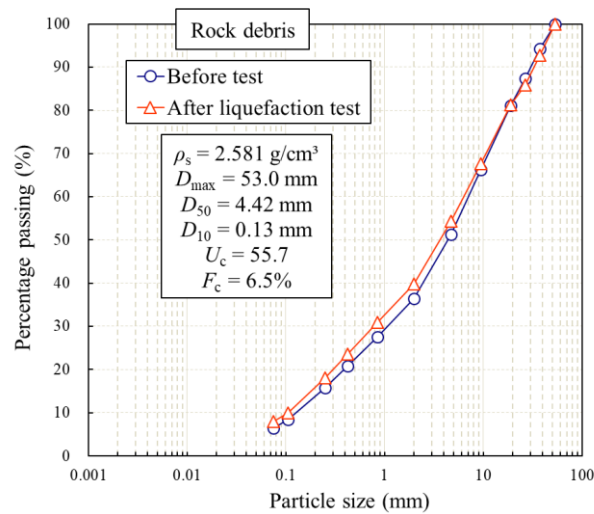
2

Figure 1 – Particle size distribution and basic properties of the test samples

2.2 Test Apparatus and Procedure

The laboratory tests were conducted using a large triaxial apparatus. The initial specimen diameter and height were 300 mm and 600 mm, respectively. This diameter is larger than the maximum particle size (D_{max}) of the rock debris by more than a factor of 5, which is necessary to conduct suitable tests for granular materials with U_c value of more than 5 in accordance with the JGS 0530-2009.

After setting the specimen in the triaxial cell, the specimen was filled with CO_2 gas through the void between the particles and then saturated with de-aired water. Back pressure was applied until the pore water pressure coefficient (B value) is higher than 0.95. The back pressure was 200 kPa except for the triaxial compression tests under undrained conditions (400 kPa in these tests). The specimen was isotropically consolidated at a given confining pressure. This procedure was performed for each test.

The triaxial compression test was conducted under drained and undrained conditions at an axial strain rate of 0.05%/min until the axial strain reaches 15%. The effective confining pressure (σ'_c) values were 25 kPa, 50 kPa, 100 kPa, and 150 kPa under drained conditions, and 50 kPa and 100 kPa under undrained conditions. The pore water pressure was measured under undrained conditions.

The cyclic deformation test was conducted under undrained conditions using sine waves at a frequency of 0.01 Hz. The σ'_c value was 50 kPa or 100 kPa.

The undrained cyclic loading test was conducted using sine waves at a frequency of 0.01 Hz. The σ'_c value was 50 kPa or 100 kPa. Cyclic loading was generally continued until the double amplitude strain (ε_{DA}) exceeds 5%. Cyclic loading was stopped in several tests when ε_{DA} exceeds 2% or 3.5% to limit the strain history. The volumetric strain (ε_v) generated as a result of reconsolidation after undrained cyclic loading was measured by opening the valve after each test.

In a large triaxial test, there is a concern regarding the uniformity of the specimen; the development of pore water pressure may vary between the edge of the specimen and the center of the specimen. Thus, a preliminary liquefaction test was conducted to confirm uniform development of the pore water pressure. A pore water pressure gauge was placed in the center of the specimen at a height of 300 mm from the side of the specimen. The back pressure was measured both at the top and bottom of the specimen. Figure 2 shows the results of the preliminary test. The excess pore water pressure ratio ($\Delta u/\sigma'_c$) was almost the same in the three measured values. Therefore, the uniformity of the specimen as an element test is established in this study.
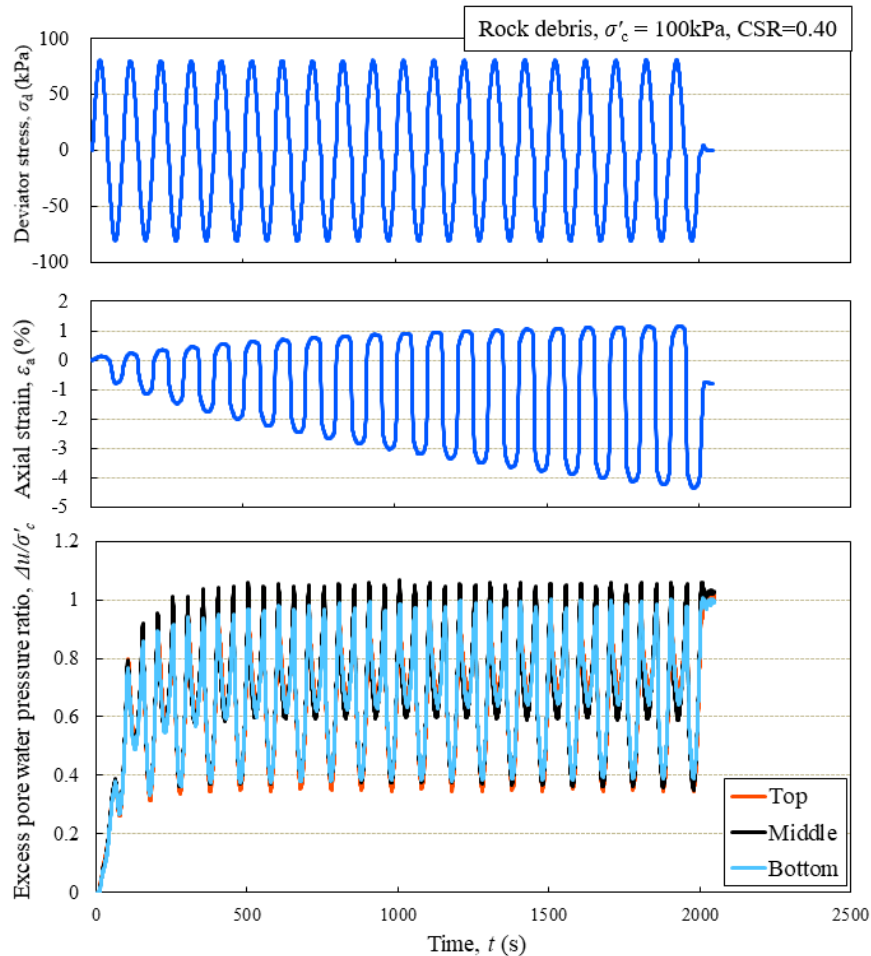
3

Figure 2 – Deviator stress, axial strain, and excess pore water pressure ratio results of the preliminary test

3. Results

3.1 Triaxial Compression Test

Figure 3 shows the stress–strain relationship of the triaxial compression tests under drained and undrained conditions. Strain softening and positive dilatancy was observed under drained conditions. The axial strain corresponding to the peak shear strength increased at higher confining pressures. Negative pore water pressure was observed under undrained conditions, indicating that the rock debris has similar dilatancy characteristics as dense sand. The degree of positive dilatancy became less as the confining pressure increased under both drained and undrained conditions.

Figure 4 shows the effective stress path under undrained conditions. The rock debris exhibited dilative behavior after reaching the phase transformation line. Steady state was not observed within an axial strain of 15%.

Figure 5 shows the Mohr's stress circle at failure under drained conditions. The value of the internal friction angle (φ_d) for the tested rock debris is 43.7°, which is within the range of a typical value for gravel [6].

4

(a)   (b)

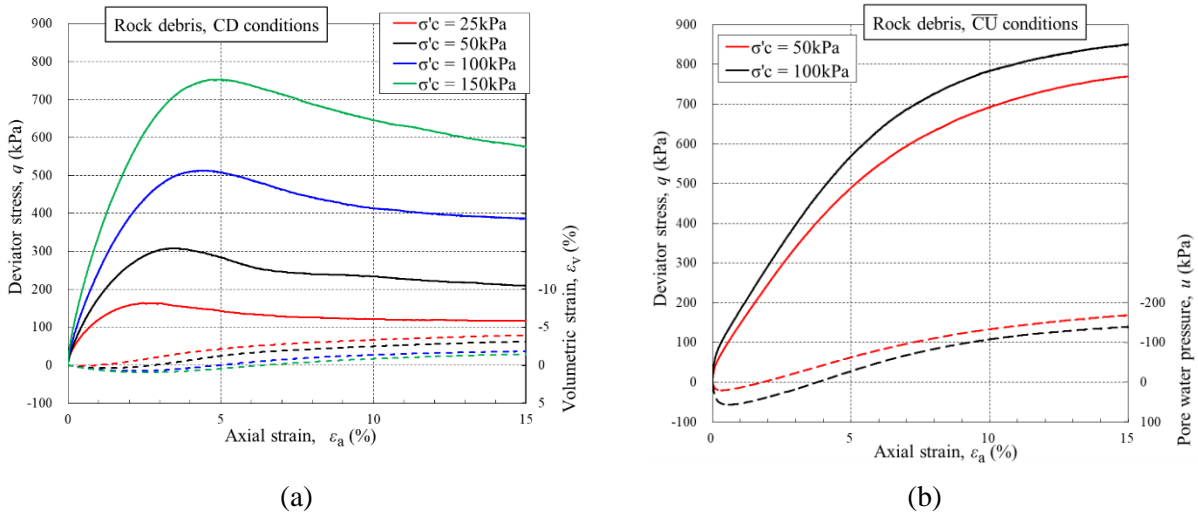Figure 3 – Stress–strain relationship in triaxial compression test under (a) consolidated drained (CD) conditions and (b) consolidated undrained ($\overline{CU}$) conditions
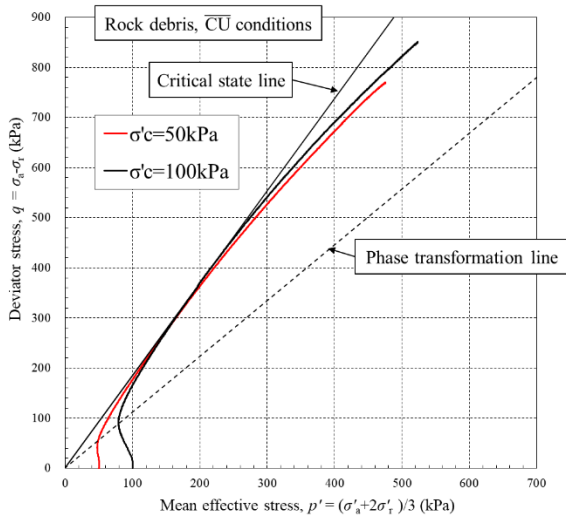

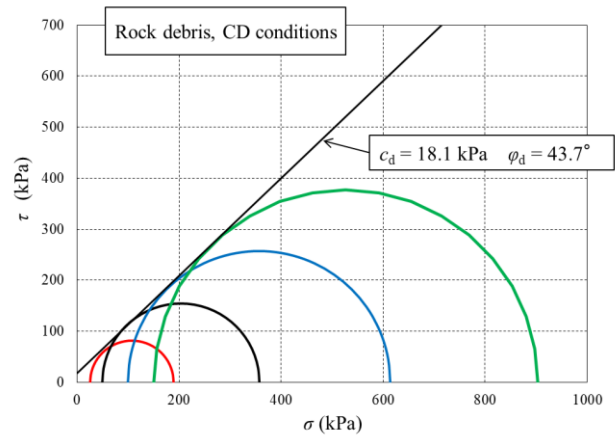Figure 4 – Effective stress path in triaxial compression test under consolidated undrained ($\overline{CU}$) conditions

Figure 5 – Mohr's stress circle under consolidated drained (CD) conditions

3.2 Cyclic Deformation Test

Figure 6 shows the variations of the shear modulus (G), damping ratio (h), and shear modulus ratio (G/G_0) with the shear strain (γ). It can be observed that the γ–G/G_0 and γ–h relationships are almost the same at different confining pressures.

5

(a)

(b)
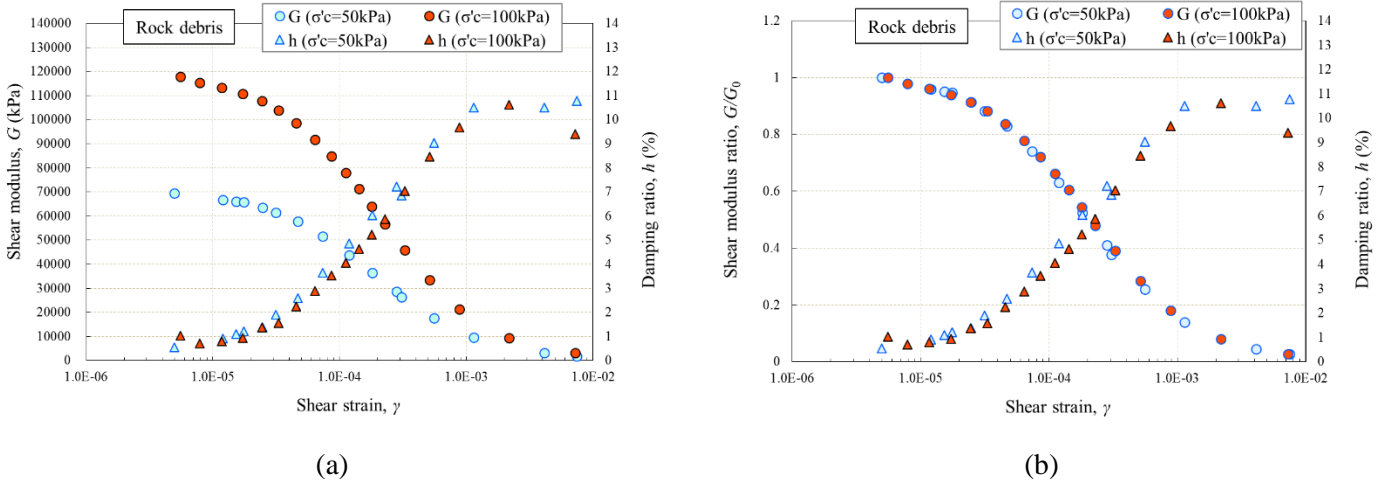
Figure 6 – Relationships between γ–h and (a) γ–G and (b) γ–G/G_0

3.3 Undrained Cyclic Loading Test

Figure 7 shows a typical example of the effective stress path and the stress–strain relationship during undrained cyclic loading (effective confining pressure, σ'_c = 100 kPa and cyclic stress ratio, CSR = 0.50). Cyclic mobility was observed in each test; the axial strain gradually increased even after the mean effective stress (p') became zero because the effective stress recovered as a result of shearing by positive dilatancy. The development of the axial strain shifted to the extension direction (negative value).

Figure 8 shows the liquefaction resistance curve. The effect of system compliance (membrane penetration) during cyclic loading was evaluated using the simplified method proposed by Tokimatsu [7]. The system compliance ratio (C_R) was 0.40 at σ'_c value of 100 kPa and 0.18 at σ'_c value of 50 kPa. The C_R was evaluated by the test conducted using the lowest CSR at different σ'_c values. The liquefaction resistance (R_L) values (CSR to achieve ε_{DA} of 5% at 20 cycles) were 0.29 (σ'_c = 100 kPa) and 0.40 (σ'_c = 50 kPa).
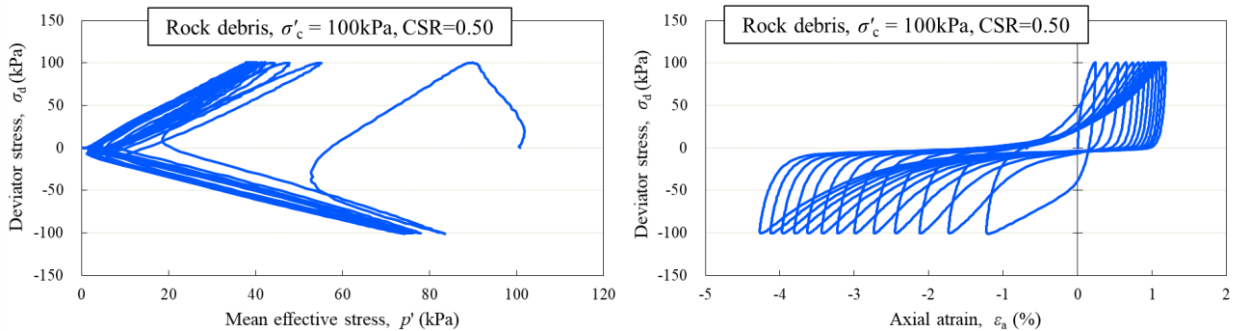

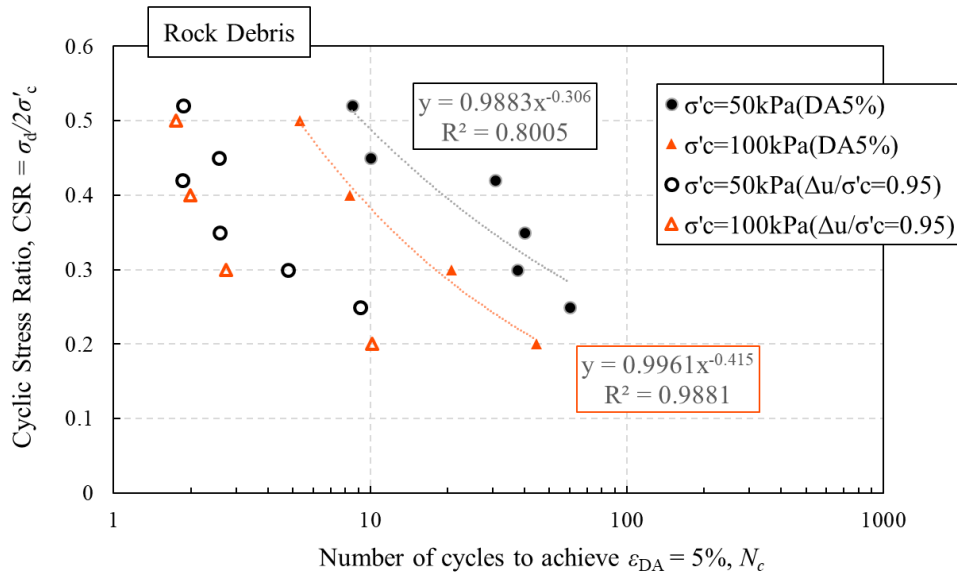Figure 7 – Effective stress path and stress–strain relationship during liquefaction test with stress control

6

Figure 8 – Liquefaction resistance curve considering membrane penetration effect

4. Discussion

Figure 9 shows the relationship between the normalized accumulated dissipated energy ($\Sigma\Delta W/\sigma'_c$) and the excess pore water pressure ratio ($\Delta u/\sigma'_c$). $\Sigma\Delta W/\sigma'_c$ is the accumulated dissipated energy ($\Sigma\Delta W$) normalized using its initial confining pressure (σ'_c). The excess pore water pressure ratio was nearly 1 when $\Sigma\Delta W/\sigma'_c$ was in the range of 0.02–0.04. This result is consistent with those obtained from a previous study using clean sand [8]. A larger CSR requires a higher $\Sigma\Delta W/\sigma'_c$ value to achieve a given $\Delta u/\sigma'_c$.

Figure 10 shows the relationship between the normalized accumulated dissipated energy ($\Sigma\Delta W/\sigma'_c$) and the axial amplitude strain (ε_{DA}). The results of the undrained cyclic loading tests for Holocene sand, which was liquefied by the 2011 Great East Japan earthquake, are also shown in this figure. The liquefaction resistance (R_L) of the sand is in the range of 0.14–0.20 [9]. The increase in ε_{DA} for the normalized accumulated dissipated energy of the rock debris is small compared with that of sandy soil. The development of the axial strain depends on CSR regardless of the value of σ'_c; a larger CSR resulted in less $\Sigma\Delta W/\sigma'_c$ to achieve a given ε_{DA}. A larger CSR leads to a higher extension stress and requires less energy for strain development.

Figure 11 shows the relationship between the number of cycles (N_c) and the normalized accumulated dissipated energy ($\Sigma\Delta W/\sigma'_c$) at the liquefaction state ($\varepsilon_{DA} = 5\%$). $\Sigma\Delta W/\sigma'_c$ increased as N_c increased. This trend is different from the trend reported in a previous study that conducted torsional shear tests using sand; $\Sigma\Delta W/\sigma'_c$ was almost constant even when N_c increased [8]. Figure 12 shows the relationship between R_L and $\Sigma\Delta W/\sigma'_c$ to achieve $\varepsilon_{DA} = 5\%$ at $N_c = 20$. The proposed equation for R_L formulated using the stress-based method and $\Sigma\Delta W/\sigma'_c$ based on element tests for sandy soil [8] is shown in the figure. The results obtained using the tested rock debris seem to underestimate the R_L value based on the $\Sigma\Delta W/\sigma'_c$. A possible reason is the inclination of strain development to the extension direction, which leads to less N_c to achieve ε_{DA} of 5% at a large CSR. The asymmetry of the strain due to the extension stress is a limitation of the triaxial apparatus. Further research is necessary to mitigate the effect of stress asymmetry.
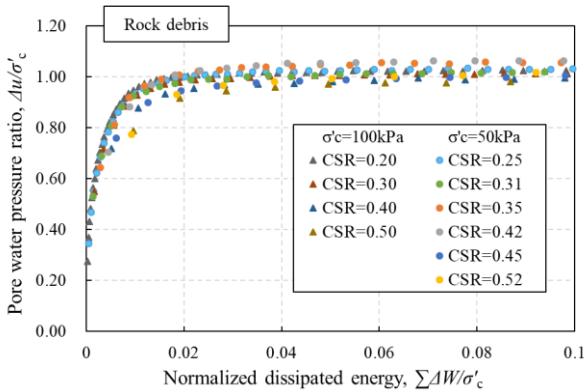
7

Figure 9 – Relationship between normalized accumulated dissipated energy and excess pore water pressure ratio
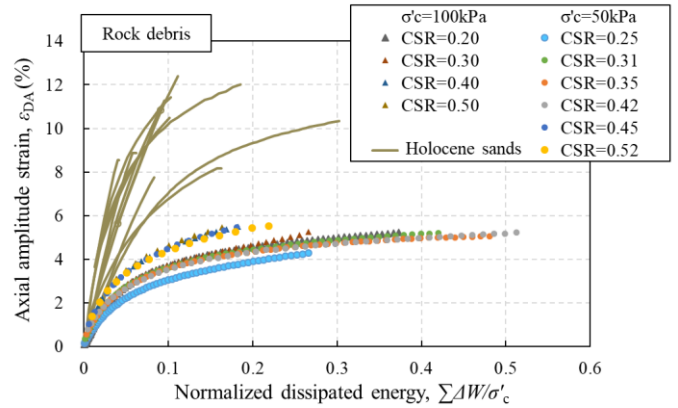

Figure 10 – Relationship between normalized accumulated dissipated energy and maximum axial strain (modified based on [9])
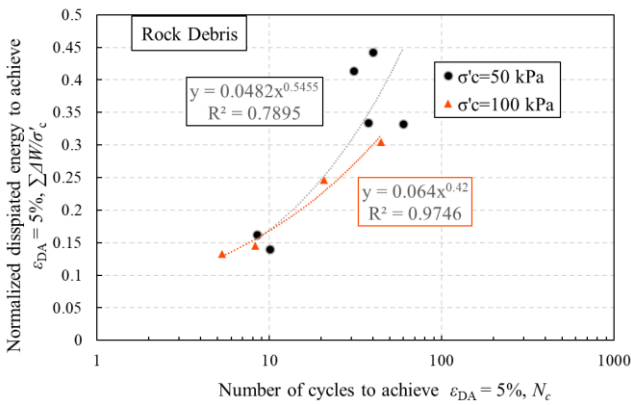

Figure 11 – Relationship between number of cycles and normalized accumulated dissipated energy
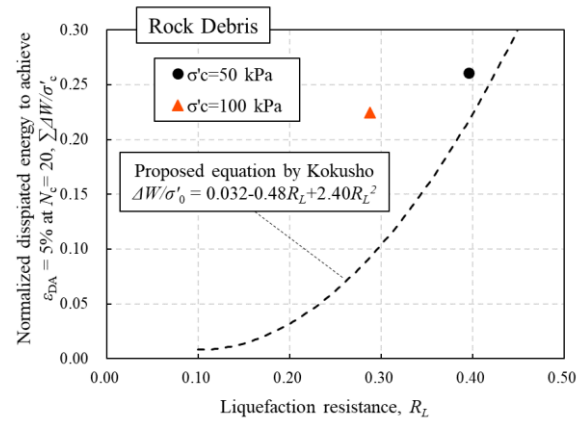

Figure 12 – Relationship between liquefaction resistance and normalized accumulated dissipated energy [8]

Figure 13 shows the relationship between the maximum axial amplitude strain (ε_{DA}) and the shear modulus ratio (G/G_{max}), whereas Figure 14 shows the relationship between the normalized dissipated energy and ($\Sigma\Delta W/\sigma'_c$) and G/G_{max}. The secant shear modulus (G) is the slope of the line connecting the two points of the hysteresis loop for each cyclic loading. The maximum shear modulus (G_{max}) is defined as the maximum G for each test. Both ε_{DA}–G/G_{max} and $\Sigma\Delta W/\sigma'_c$–G/G_{max} depend on CSR; a higher CSR will likely result in a higher G/G_{max} at a given ε_{DA} or $\Sigma\Delta W/\sigma'_c$.

Figure 15 shows the relationship between the reference strain ratio ($\gamma/\gamma_{0.5}$) and the shear modulus ratio (G/G_{max}), whereas Figure 16 shows the relationship between the reference dissipated energy ratio ($W/W_{0.5}$) and G/G_{max}. The reference strain ($\gamma_{0.5}$) and the reference dissipated energy ($W_{0.5}$) are the strain and energy at $G/G_{max} = 0.5$, respectively. The $\gamma/\gamma_{0.5}$–G/G_{max} relationship is almost the same regardless of the CSR value, which is consistent with the results obtained by Nishi et al. [10] using soft rock. On the other hand, the $W/W_{0.5}$–G/G_{max} relationship still depends on the CSR value; a higher CSR will likely result in a higher G/G_{max} at a given $W/W_{0.5}$.
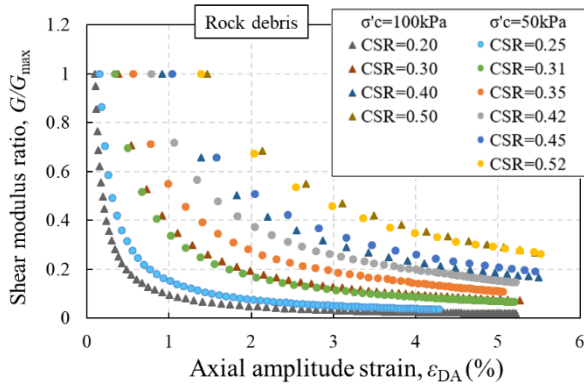
8

Figure 13 – Relationship between ε_{DA} and shear modulus ratio
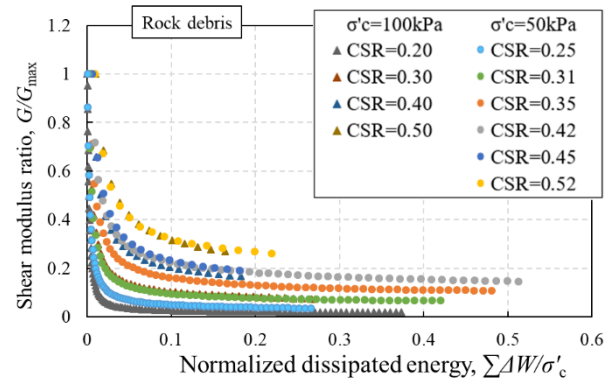

Figure 14 – Relationship between normalized accumulated dissipated energy and shear modulus ratio
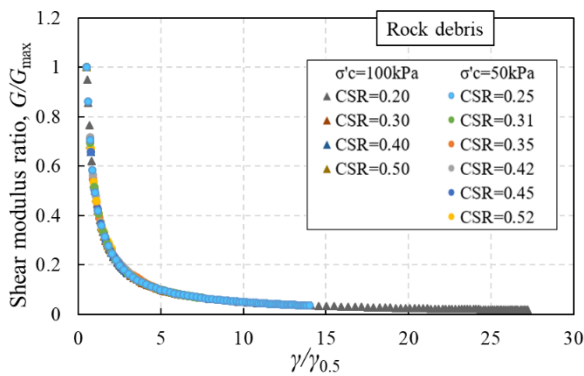

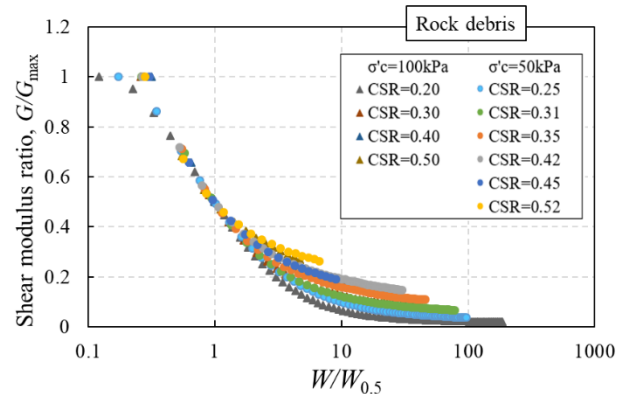Figure 15 – Relationship between reference strain ratio and shear modulus ratio

Figure 16 – Relationship between $W/W_{0.5}$ and G/G_{max}

Figure 17 shows the relationship between the maximum shear strain (γ_{max}) and the volumetric strain as a result of reconsolidation after liquefaction (ε_v). "Average" represents a power trendline of the rock debris under σ'_c = 50 kPa and σ'_c = 100 kPa. The results reported by Tanaka et al. [11] using undisturbed gravelly samples are also shown in the figure. Although γ_{max} > 10% was not obtained owing to experimental limitation, a larger γ_{max} resulted in a larger ε_v, which is consistent with results obtained by Ishihara and Yoshimine [12] using clean sand.

Figure 18 shows the relationship between the accumulated shear strain ($\Sigma|\Delta\gamma|$) and ε_v. The value of ε_v increased with the increase in $\Sigma|\Delta\gamma|$, which is consistent with results obtained by Unno et al. [13] using clean sand.

Figure 19 shows the relationship between the normalized accumulated dissipated energy ($\Sigma\Delta W/\sigma'_c$) and ε_v; ε_v increased with the increase in $\Sigma\Delta W/\sigma'_c$. In terms of the coefficient of determination (R^2) of the power trendlines, the $\Sigma\Delta W/\sigma'_c$–ε_v relationship has a higher R^2 than those of $\Sigma|\Delta\gamma|$–ε_v and γ_{max}–ε_v relationships, which indicates that the energy-based method can evaluate the post-liquefaction behavior of rock debris more accurately.
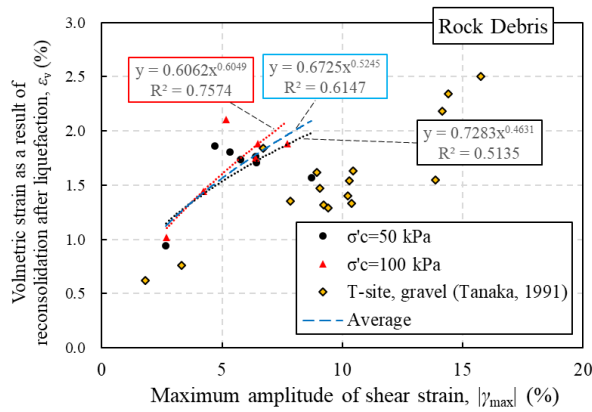
9

Figure 17 – Relationship between the maximum shear strain and volumetric strain as a result of reconsolidation after liquefaction (modified based on [11])
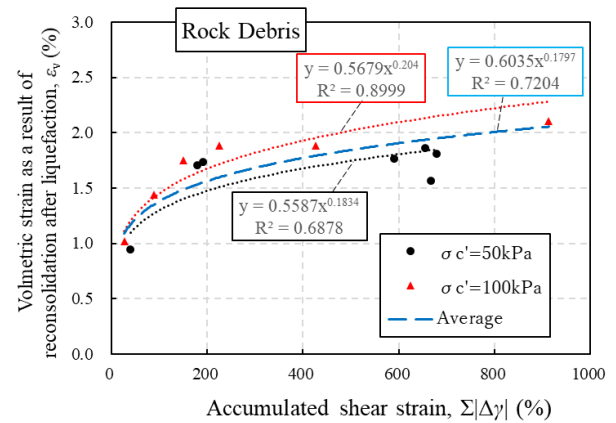

Figure 18 – Relationship between the accumulated shear strain and volumetric strain as a result of reconsolidation after liquefaction
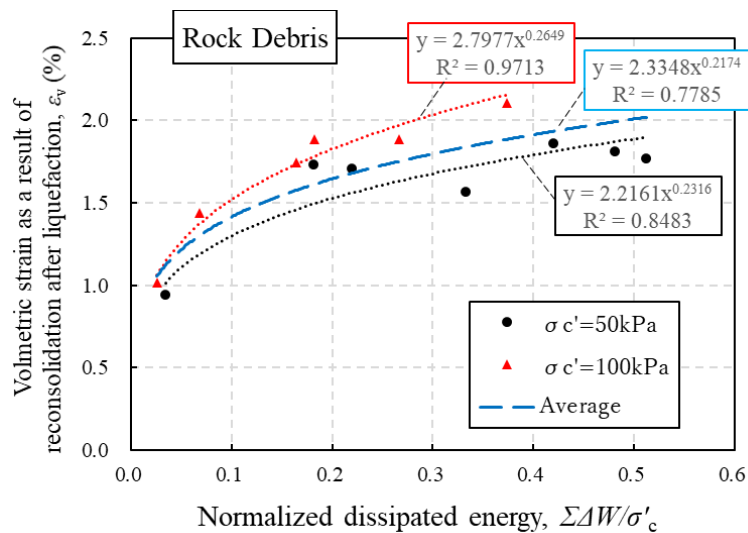

Figure 19 – Relationship between the accumulated shear strain and volumetric strain as a result of reconsolidation after liquefaction

5. Conclusion

In this study, a series of large triaxial tests were conducted for rock debris using a large triaxial apparatus (300 mm in diameter and 600 mm in height) to clarify the applicability of the energy-based method to rock debris. The following conclusions are drawn based on the findings of this study.

1. In a large triaxial test using rock debris, the development of pore water pressure was uniform in the specimen; the pore water pressure at the center of the specimen was almost the same as that at the edge of the specimen.

10

2. The excess pore water pressure ratio was nearly 1 when the normalized accumulated dissipated energy ($\Sigma\Delta W/\sigma'_c$) reached 0.02–0.04, which is consistent with results obtained using sandy soil. On the other hand, the strain development and R_L for $\Sigma\Delta W/\sigma'_c$ were small compared with those of sandy soil.

3. The cyclic stress ratio (CSR) had an influence on the relationship between the normalized accumulated dissipated energy and the shear modulus ratio (G/G_{max}) even when normalization was performed.

4. The volumetric strain as a result of reconsolidation after liquefaction (ε_v) has a stronger relationship with the normalized accumulated dissipated energy compared with the maximum shear strain (γ_{max}) or the accumulated shear strain ($\Sigma|\Delta\gamma|$). This indicates that the energy-based method can evaluate the post-liquefaction behavior of rock debris more accurately.

In this study, the effect of stress asymmetry on strain development was observed. Further research, such as model testing, is necessary to mitigate this effect.

6. References

[1] Kokusho T, Tanaka Y, Kawai T, Kudo K, Suzuki K, Tohda S, Abe S (1995): Case study of rock debris avalanche gravel liquefied during 1993 Hokaido-Nansei-Oki Earthquake. *Soils and Foundations*, **35** (3), 83-95.

[2] Hatanaka M, Uchida A, Ohara J (1997): Liquefaction characteristics of gravelly fill liquefied during the 1995 Hyogo-Ken Nanbu Earthquake. *Soils and Foundations*, **37** (3), 107-115.

[3] Hara T, Kokusho T, Hiraoka R (2004): Undrained strength of gravelly soils with different particle gradations, *13ᵗʰ World Conference on Earthquake Engineering*, Paper No. 144, Vancouver, Canada.

[4] Towhata I, Ishihara K (1985): Shear work and pore water pressure in untrained shear. *Soils and Foundations*, **25** (3), 73–84.

[5] Ricardo J.N. Azeiteiroa, Paulo A.L.F. Coelhoa, David M.G. Tabordab, José C.D. Grazinaa (2017): Energy-based evaluation of liquefaction potential under non-uniform cyclic loading. *Soil Dynamics and Earthquake Engineering,* 92, 650-665.

[6] JGS committee on physical properties of gravelly soils (2001): Technical status report on physical properties of gravelly soils. *JGS Symposium on physical properties of gravelly soils*, 1-149. (in Japanese)

[7] Tokimatsu K (1990): System compliance correction from pore pressure response in undrained cyclic triaxial tests. *Soils and Foundations*, **30** (2), 14-22.

[8] Kokusho T (2013): Applicability of energy-based liquefaction potential evaluation method compared with FL-method. *Japanese Geotechnical Journal*, **8** (3), 463-475. (in Japanese)

[9] JGS committee on liquefaction evaluation method based on energy (2019): Action report on liquefaction evaluation method based on energy. *JGS Symposium on liquefaction evaluation method based on energy*, 1-202. (in Japanese)

[10] Nishi K, Ishiguro T, Kudo K (1989): Dynamic properties of weathered sedimentary soft rocks. *Soils and Foundations*, **29** (3), 67-82

[11] Tanaka Y, Kudo K, Yoshida Y, Kokusyo Y (1991): Evaluation method of dynamic strength and residual settlement for gravelly soils. *Research report of Central Research Institute of Electric Power Industry*, U90063. (in Japanese)

[12] Ishihara K, Yoshimine M (1992): Evaluation of settlements in sand deposit following liquefaction during earthquakes. *Soils and Foundations*, **32** (1), 173−188.

[13] Unno T, Kazama M, Uzuoka R, Sento N (2006): Relation of volumetric compression of sand between under drained cyclic shear and reconsolidation after undrained cyclic shear. *Journal of Japan Society of Civil Engineers, Ser. C (Geosphere Engineering)*, **62** (4), 757-766. (in Japanese)